POLITECNICO
DI TORINO

Université
de Paris

International Master Course in Nanotechnologies and Quantum Devices

Master Degree Thesis

Optimization of an optical setup for the measurement of single photons emitted by a quantum dot

Simulation of micropillar cavity coupling to a fiber and investigation of technologies for telecom single-photon sources

Supervisors
Prof. Carlo Ricciardi
Prof. Maria Luisa Della Rocca

Candidate
Nico Margaria

Internship Tutor
Quandela (spinoff C2N)
Dr. Niccolo Somaschi

July 2020

Acknowledgements

I want to express my gratitude to the whole Quandela team for their support, and to Huong and Pascale for the training and collaboration for the simulations.

I also congratulate with my fellow NanoQuad students, with which we shared so many experiences in Paris.

Finally I must thank my longtime friends, my family, and my girlfriend, that even if distant were always with me.

Contents

1 Introduction

1.1 Context

The internship took place in Quandela, a start-up based in the Center for Nanoscience and Nanotechnology (C2N). The Quandela team develops unique technologies for the fabrication of increasingly high-performance quantum light sources based on semiconductor quantum dots (QD). These efficient sources are useful for multiple strategic applications such as optical quantum computing, quantum communications, and quantum light-based imaging and detection.
The team has also an active collaboration with the group of Pascale Senellart (co-founder of Quandela) for simulations, fabrication, and experiments.

At present, most of the sources used for quantum communications are based on non-linear crystals, in which pairs of photons are generated probabilistically from a laser pulse. They are useful for entanglement and QKD protocols (the presence of a herald photon ensures sending of the signal), but are not efficient and rely on non-deterministic processes.
Efficient and high-quality single-photon sources are fundamental for the advancement of optical quantum technologies and quantum communications. Solid state sources based on semiconductor QDs in microcavities are very promising for the emission rate at which they can be pushed and on their true on-demand nature.
The applications of single-photons sources based on self-assembled QDs can be organized on the basis of different characteristics (properly defined later on). For their brightness they are used in sensing, for their purity they allow safe communication[1] and for their indistinguishability they are useful in quantum algorithms and quantum repeaters.

The first weeks of the internship were spent in learning and assimilating the techniques and analyses used in the characterization of the sources, together with the instrumentation used in the lab. The initial plan of performing experiments have been adapted to the limited possibilities during the lockdown. The training has moved from the lab to a simulation software. In parallel the bibliography has been even more important in the learning method. First of all it was necessary to understand the basics of the present single-photon sources technology. The goal was accomplished through discussions and a bibliographic work both on papers of the group and the alternatives used in this continuously advancing field.

In this stimulating context, the work described in this report is aimed at facing different challenges, such as improving the collection efficiency through the simulation of direct fiber coupling of the sources and laying the groundwork to future advancements toward the telecom range.

Before going into the details of the work, the basics of single-photon sources and a few possible implementations are briefly described.

[1] not yet at the right wavelength, but some options are under study and are part of this report

1.2 Introduction to single-photon sources and state of the art

Before focusing on any particular system, it is instructive to define what are the properties that are required for a single-photon source to be used for quantum information, computation or cryptography applications.
With that in mind, here are described the parameters to characterize a generic single-photon source, in particular the focus is on purity, indistinguishability, and brightness, with an idea of how to quantify and measure each one.

Single-photon sources figures of merit [1]

An ideal single-photon source is expected to produce on-demand one (and only one) photon in a pure quantum state. In practice, to characterize these properties of interest, one measures three main figures of merit: the purity, the indistinguishability and the brightness.

- **Purity** characterizes the ability of the emitter to produce not more than one photon in each pulse. The parameter carrying this information is the second order correlation function at zero delay $g^{(2)}(0)$ measured through a Hambury-Brown and Twiss setup.
  As shown in Figure 1, it is made of a beam splitter (BS) and two single-photon detectors. Having only one input, any coincidence in the detectors reveals that more than one photon was emitted.
  The $g^{(2)}(0)$ of an ideal single-photon source is 0. For comparison with other kinds of sources, in coherent laser sources the arrival of a photon is independent from the others thus $g^{(2)}(0)=1$, for thermal sources instead photons bunch together, leading to $g^{(2)}(0)=2$.

  Referring to the plot in Figure 1, $g^{(2)}(0)$ is computed as the integrated coincidences around zero delay normalized by the area of the side-band peaks (that are just due to single photons emitted in different pulses).

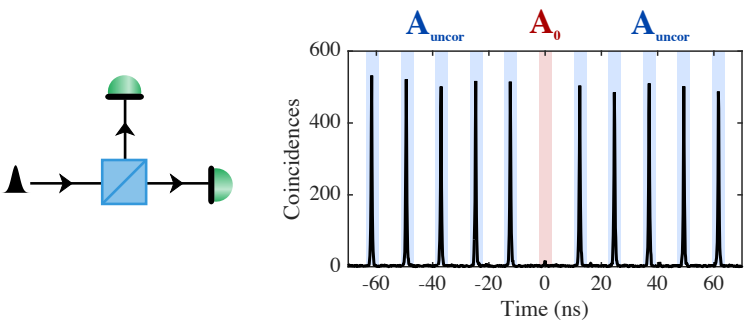

Figure 1: Characterization of the purity of single photons from a pulsed source: sketch of the HBT setup and coincidence counts as a function of time delay, from [2].

- **Indistinguishability** is achieved when photons are wavepackets that are pure[2] quantum states and not statistical mixtures. The indistinguishability of two photons is quantified by the mean photon wavepacket overlap and it is measured through Hong Ou Mandel (HOM) interference (Figure 2). This could work both between different sources and between photons that are successively emitted by the same source. The latter needs a delay, realized in a path-unbalanced interferometer.
  In general photons arriving together to a BS have the same probability of taking any path. But if the photons are indistinguishable, then there is destructive interference between the probability amplitudes of the outcomes in which photons go to a different detector, leaving photon bunching as the only option.

  The value characterizing the indistinguishability is the visibility of the HOM dip. In a pulsed regime, in which the curve is not continuous but an envelope over peaks separated in time (plot in Figure 2), the visibility of the quantum interference is written in terms of the ratio of the coincidences at zero delay (A_0) and the averaged coincidences of the uncorrelated peaks[3] (A_{uncor}). In formula $V_{HOM} = 1 - 2\frac{A_0}{A_{uncor}}$.

  V_{HOM} can be corrected for not ideal purity (knowing that in practice $g^{(2)}(0) \neq 0$), in order to characterize the wavepacket overlap for all degrees of freedom other than photon number. For sufficiently small $g^{(2)}(0)$ the intrinsic indistinguishability is $V^*_{HOM} = \frac{V_{HOM}+g^{(2)}(0)}{1-g^{(2)}(0)}$ [2]. Separating the two aspects allows a more precise diagnosis of imperfect single-photon sources. Still the relevant parameter for applications remains V_{HOM}.

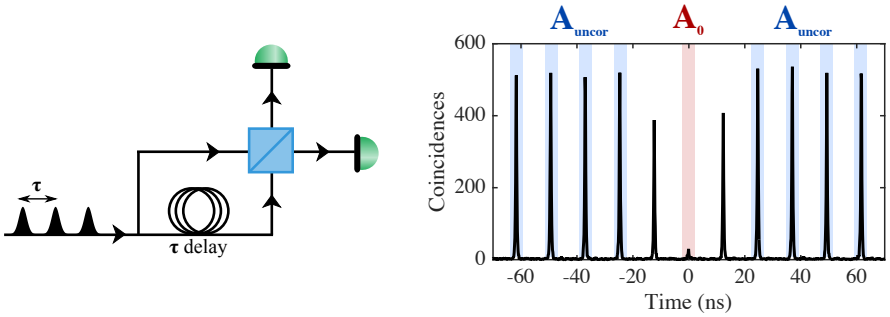

Figure 2: Characterization of the indistinguishability of single photons from a pulsed source: sketch of the HOM setup and coincidence counts as a function of time delay, from [2].

- **Brightness** is the average amount of photons collected per excitation pulse. The definition is not too specific to be able to compare different sources.
  The first-lens brightness, together with the source repetition rate, the transmission of the optical network, and detector efficiencies, will give the rate at

[2]Here with another acceptation with respect to the purity described just before
[3]Obtained excluding the two peaks around the cental one, which are still part of the HOM dip.

which single photons can be made available at the output (e.g. a single mode fiber). This, in turn, determines the speed of quantum communications or computation protocols.
For practical purposes also the fibered brightness can be defined, that is the brightness measured after collection into a monomode fiber.

The scalability of the number of identical photons (produced by demultiplexing or using identical sources) is strongly dependent on the brightness of the source. The lack of scalable single-photon sources has become one of the major roadblocks in the development of quantum photonics[4].

Alternative interpretation of purity and brightness in the Fock basis
Another point of view may be useful to better understand the meaning and importance of these figures of merit. This is done by writing the state of the emitted pulse as a statistical mixture of different Fock states

$$|\psi\rangle = p[0]\ |0\rangle + p[1]\ |1\rangle + p[2]\ |2\rangle + ...;\ \sum_{i=0}^{+\infty} p[i] = 1$$

with coefficients $p[i]$ being the probabilities of having i photons.

A simplified interpretation of $g^{(2)}(0)$ is found neglecting the contributions of pulses with more than two photons. This is reasonable since the considered sources have, to be defined of single photons, negligible probability of emitting a large number of photons together.
Formally, in terms of the number operator and at zero delay [3]

$$g^{(2)}(0) = \frac{\langle n^2(t) - n(t)\rangle}{\langle n(t)\rangle^2} = \frac{\langle n^2(t)\rangle - \langle n(t)\rangle}{\langle n(t)\rangle^2}$$

The expectation values of interest can be rewritten by decomposition in the Fock basis, resulting in the weighted sums

$$\langle n(t)\rangle = 0 \cdot p[0] + 1 \cdot p[1] + 2 \cdot p[2] + ...$$

$$\langle n^2(t)\rangle = 0 \cdot p[0] + 1 \cdot p[1] + 4 \cdot p[2] + ...$$

thus giving

$$g^{(2)}(0) = \frac{\cancel{p[1]} + 4 \cdot p[2] + ... - (\cancel{p[1]} + 2 \cdot p[2] + ...)}{p^2[1] + 2 \cdot p^2[2] + ...} \simeq \frac{2 \cdot p[2]}{p^2[1]}$$

where the last step is valid making the approximation $p[1] \gg p[2] \gg p[> 2]$.

The interpretation of the brightness is more simply the probability of having a pulse with no vacuum component. That corresponds to $p(1)$ for $p(1) \gg p(> 1)$.
In practice, having no vacuum component is difficult to achieve since any optical

[4]The other key actors in this context are efficient linear circuits and single-photon detectors.

component introduces losses, with an increase of the vacuum contribution. This must be considered when one calculates the number of emitted photons per unit of time.
After this brief introduction it is possible to describe how different devices are able to satisfy those requirements and compare a few available options.

From nonlinear crystals to QD-based single-photon sources [1, 4]

For a long time single-photon-based technologies (like optical quantum communications and computation protocols) have used heralded single-photon sources, relying on probabilistic photon pair generation in $\chi^{(2)}$ or $\chi^{(3)}$ non-linear crystals. The name "heralded" has its roots in the detection of one photon of the pair assuring the presence of the other one.
An intrinsic limitation of exploiting non-linearities is that a compromise arises between brightness and purity. The frequency conversion is probabilistic and sending more photons in the non-linear crystal results in an increased probability of generating two pairs. To avoid this and to preserve the purity, most of the excitation pulses end up with no photon pairs at all. As a consequence, reaching high efficiencies requires difficult multiplexing schemes.

In contrast, in recent years a new kind of on-demand single-photon sources has emerged. While offering very high quality photons in terms of purity and indistinguishability, the brightness of those sources is much larger. The actual values of the brightness[5] depend on many details not covered here like: where it is measured (at the first lens or into a fiber), what structure is used, the technique of excitation (in/near/off resonance or exploiting phonons), and others.

To obtain such features, sources based on QDs in microcavities are used. There exist different designs such as 2D photonic crystals, microdisks, and micropillars. A complete description of the possible implementations is given in [7].

1.3 Description of single-photon sources based on semiconductor QDs in micropillars

What follows is an introduction of the physical and technological concepts of the single-photon sources Quandela produces and is working on.

Energy levels of QDs

The core of the emitter is a InAs QD surrounded by GaAs. .. Because of the lower energy bandgap of the former with respect to the latter, a QD of this kind can confine electrons and holes. Due to the small dimensions in all directions, charged

[5]For example in [5] have 60% polarized first-lens brightness under resonant excitation. In [6] have >75% first-lens brightness.

particles in the QD will occupy discrete energy levels. A simplified picture of the possible excited states of QDs is shown in Figure 3.

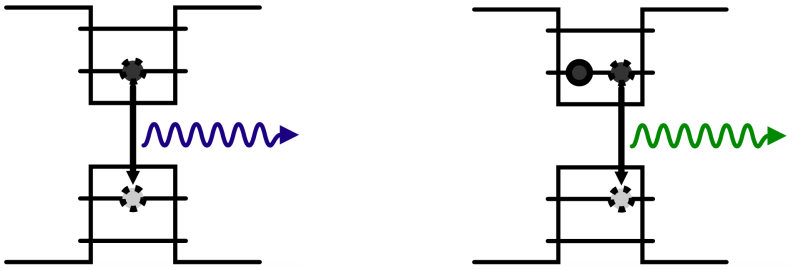

(a) Sketch of exciton energy levels (one electron-hole pair)

(b) Sketch of trion energy levels (one electron-hole pair + one charge)

Figure 3: Simplified view of the energy levels of QDs, from [8]

The physics behind the interpretation of the levels includes the effects of carrier localization and Coulomb and exchange interactions. Those lead to excitonic many-body states with lifted degeneracies and particular selection rules. For the sake of simplicity, here QDs are considered as behaving like artificial atoms (two-level systems) when concentrating on a particular energy.
One way to populate coherently the QD is the so-called resonant excitation. Sending a laser pulse at the same energy as the exciton/trion transition results in a single excitation, thus can emit single photons on demand.
Moreover, as discussed in the following, by fabricating a microcavity around a QD, these single photons can be efficiently emitted and collected. This is needed since QDs alone have non-directional emission and total internal reflection in the semiconductor limits the light able to escape. For example in bulk samples the collection efficiency is $\approx 1\%$.

The role of the cavity: enhancement by Purcell effect

Designing a proper optical cavity around the QD it is possible increase its coupling to a particular optical mode, thus increasing the spontaneous emission rate. This is possible because spontaneous emission is not an intrinsic property of the emitter and can be enhanced or reduced in different spectral ranges by the electromagnetic modes it can emit into (Purcell effect). Some conditions must be satisfied for this to work, like the QD being placed at the confined optical field maximum and one of its transitions to be in spectral resonance with the cavity.

In this kind of cavities the emission rate of a QD in the cavity mode is accelerated by a factor F_p while the rate into other modes is unchanged. As a consequence the probability of emission into the desired mode is $\frac{F_p}{1+F_p}$, that is intuitively the ratio of favorable cases to all cases.

Link to cavity QED

From the point of view of cavity quantum electrodynamics, the considered case falls

in the weak coupling regime, meaning that the QD (as a two-level system) and the cavity (as a resonator) are unlikely to periodically exchange an excitation. Initially the QD, that in this simplified view is a two-level system, is excited by an external laser pulse. When it relaxes to its ground state and emits a photon, it will not be excited again because of the (relatively) large losses of the cavity and because the pulse is over. (Included in the losses in this picture there is also the desired emission, that is on purpose favored.) On the other hand, if the cavity was made to not let the photon escape, the QD could be excited again and the cycle repeated, characteristic behavior of the strong coupling regime.
A more complete approach is done considering three rates characterizing the coupled systems: coupling, cavity losses, emission in other cavity modes. Strong and weak coupling are two limits when one rate is dominating over the others.

Fabrication of semiconductor QD single-photon sources [9]

With the description of the growth mechanisms of the QD-microcavity system it is possible to understand how the described concepts can be realized in a device.

The whole structure is made of III-V semiconductors. In particular a planar cavity made of two distributed Bragg reflectors (DBR), made of stacked pairs of AlAs and GaAs $\lambda/4$ layers, separated by a λ layer, all deposited by molecular beam epitaxy (MBE, technique that reaches atomic layer resolution) on a GaAs substrate. This structure is used to confine the states of light in the growth direction.
Particular attention is required on the step in which the QDs are formed. In the middle of the cavity deposition, a thin layer of InAs is deposited. Once it is thicker than 1.7 monolayers the stress induced by the difference in lattice constant with the underlying GaAs makes it more energy efficient for islands to form on top a remaining wetting layer, that is a continuous compressed layer of InAs. The islands are then covered with GaAs as part of the top half of the cavity and the deposition continues. The described features are clearly visible in Figure 4.

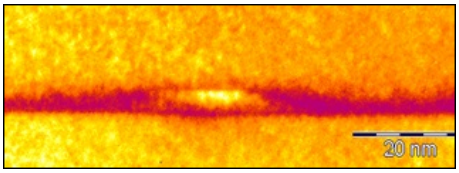

Figure 4: Transmission Electron Microscope image of the section a single InGaAs QD embedded into GaAs material. Image measured by A. Lemaitre and C. Gomez at C2N.

At this point, a planar cavity embedding randomly positioned QDs has been grown. A cryogenic in-situ lithography technique (see Figure 5) is used to deterministically dig a structure around them. The QD position is measured optically by imaging their emission pumped with a laser. A second laser line, aligned to the first, is used to define a pattern precisely centred on the QD on a predeposited photoresist.

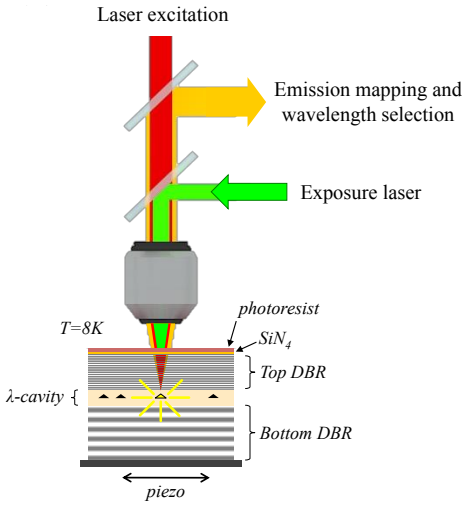

Figure 5: Scheme of the in-situ lithography, from [8].

The localization and exposure are repeated for a large number of emitters. An etching with standard techniques transfers the pattern from the photoresist to the underlying structure. With this process the diameter of the pillar is modified for its resonance to be precisely tuned with the known emission of the considered QD.

Reproducibility issues and tunability of the sources [4]
The described fabrication process allows to etch pillars centered around a QD with a precision of 50 nm. Their diameter can also be adjusted in order to have the cavity in spectral resonance with the QD.
The shape of the structures is not a simple a cylinder. In particular the pillar is connected through bridges to a circular frame and a large mesa structure where electrical contacts are attached as in Figure 6.

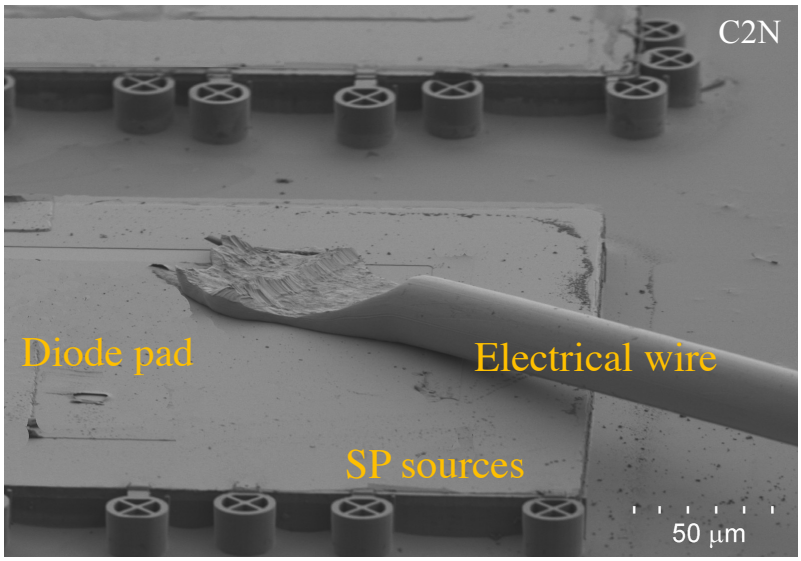

Figure 6: Scanning electron microscope image of a sample.

The structure considered here is a cylindric pillar connected by four arms to a ring used for contacting, the DBRs are gradually doped to result in a pin junction. The connected pillars have two advantages: on one side it makes possible to finely tune the QD-cavity resonance[6] via the quantum-confined Stark effect. Moreover it stabilizes the charge environment with an improvement in the indistinguishability of emitted photons.
As can be seen in Figure 7, by applying a voltage, the QD can be brought in resonance with the cavity increasing its emission rate (by Purcell enhancement as described earlier).

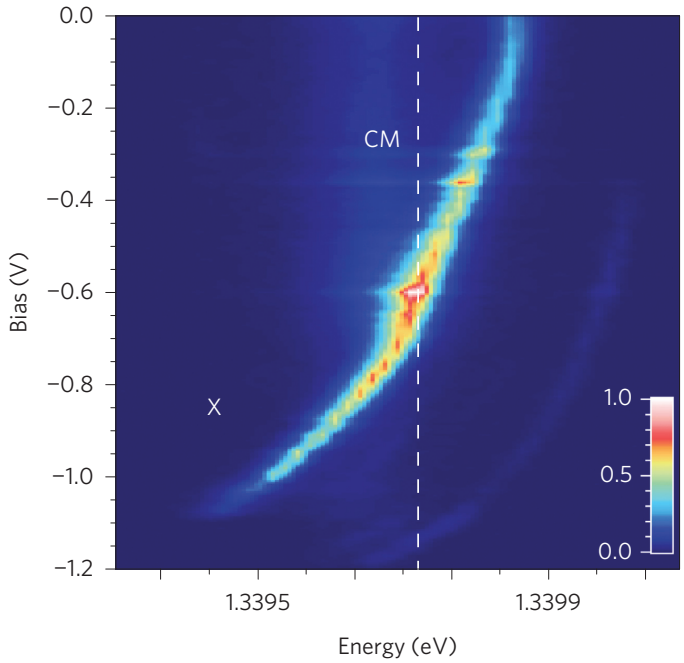

Figure 7: Emission intensity as a function of applied voltage and energy, showing the Stark tuning of the QD transition within the cavity mode (CM) resonance, from [10]

1.4 Objectives

All the work carried out during the internship have in common setting the ground for the PhD that will follow, with some limitations dictated by the absence from the laboratory[7], due to the lockdown measures.

The work has been divided in two parts, starting to address two important questions for the technology.

[6] Without this possibility, the fine tunability was done using temperature. QD-cavity resonance required to work also over 20 K. At this temperature, the interactions with the QD environment (phonons, charges,..) were detrimental for photon indistinguishability.

[7] Part of the work in the initial lab training was focused on analyzing set of data for the characterization of real sources, a summary is present in Appendix C.

- How to optimally couple a single-photon source with a monomode fiber?
- How to transfer the present technology operating at 930 nm toward the telecom range?

To deal with the fiber coupling required a basic bibliographic research but the work was mainly based on simulations on the commercial software Lumerical, with important training and practicing parts to start. The plan was to familiarize with the interface (both graphical and script) of the platform through a known example (DBR planar cavity), also aiming at understanding the potential and limitations of the simulation method.
Once learned how to perform efficient and accurate simulations, the work evolved to more complex structures simulations. Upon proper testing these pave the way to an extensive study on the effect of different structural and experimental imperfections on the coupling efficiency.
Throughout the whole process, to understand how the simulations work in general, some basics of the finite-difference time-domain method (FDTD) were needed (see Appendix A).

For what concerns the state of the art of semiconductor single-photon sources in the telecom range, the whole process was focused on bibliographic research about the most recent advancements. In parallel, the understanding of the properties of III-V semiconductors and their alloys was of great importance to get a more complete view of the problem and how it can be dealt with.

2 Coupling a QD single-photon source into a monomode fiber

The subject of this section is the study of direct coupling of a QD single-photon source into a monomode fiber placed on top of it. The reason to investigate such a system is that the current excitation/collection optical setup (Figure 8) is in free space with lenses, polarizers, and mirrors to couple the single photons into a single mode fiber using collimators. The losses are at least 40% and an improvement would greatly benefit the number of photons available at the output, thus allowing to take full advantage of the brigthness of the source.

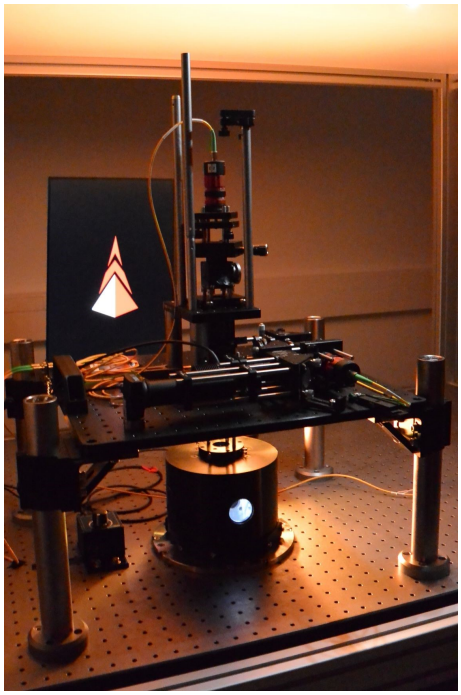

Figure 8: Picture of the experimental setup with various optical elements to couple the source to a fiber.

A picture of an alternative experimental setup is presented in Figure 9, showing a high-NA fiber over the chip in the cryostat. The sample is displaced accurately in 3D by piezos. After a first alignment of the structure, the source is ready for use.

Because of the situation that occured in spring 2020, the work performed during the internship focuses on the simulation of the system, but there is also an experimental part performed by the team. The results of the simulations, once completed, will help improving the coupling and understanding possible issues.
The simulations have been carried out using a commercial software (Lumerical), which is already in use in the group for studying the geometrical causes of losses that limit the brightness of the sources (like the diameter of the pillar or the presence of the arms used for electrical connection).

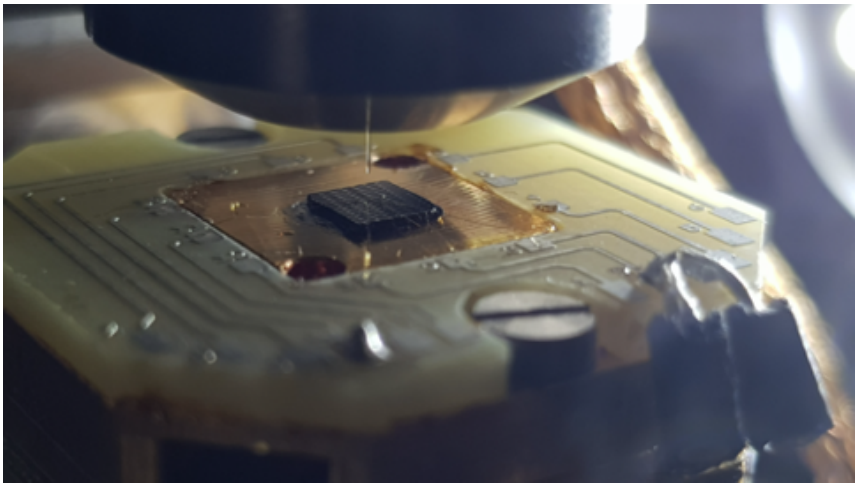

Figure 9: Picture of the experimental setup with a fiber directly coupled to a single-photon source.

In short, the optical simulation is based on the FDTD method, that consists in the solution of the Maxwell equations on a grid, including the evolution of the fields in time from sources and at the boundaries of the simulation region. For more details about the basics of FDTD refer to Appendix A.
A few advantages of this approach are the good scaling with the system size, the broadband and transient information, and its robustness and maturity. On the downside the method is not optimal for curved objects and for highly resonant devices, as will be clear in this discussion.

In general, before diving into the simulation of complex structures, it was decided to first analyze a known problem. This is of fundamental importance for checking that the simulation is working as expected. Moreover, by changing the parameters one can have an idea of the limitations of the method, in order to not encounter unexpected basic issues when dealing with problems that are yet to be successfully predicted.

2.1 FDTD simulations of a planar cavity

The first tests and simulations have dealt with the design and analysis of the very well known DBR planar cavity. Its characteristics can be found analytically, thus making it the perfect playground to practice and better learn how to deal with similar problems.

This simple system is of interest since the vertical structure is reproducing the high-Q cavity used in single-photon sources described in Section 1.3 (to be specific, in this case the structure is inspired from [11]).
The planar cavity is made of 30 DBR pairs both on the top and the bottom of the cavity. To get an idea of the system to be simulated and its relation with the pillars used in practice, two sketches are presented in Figure 10.

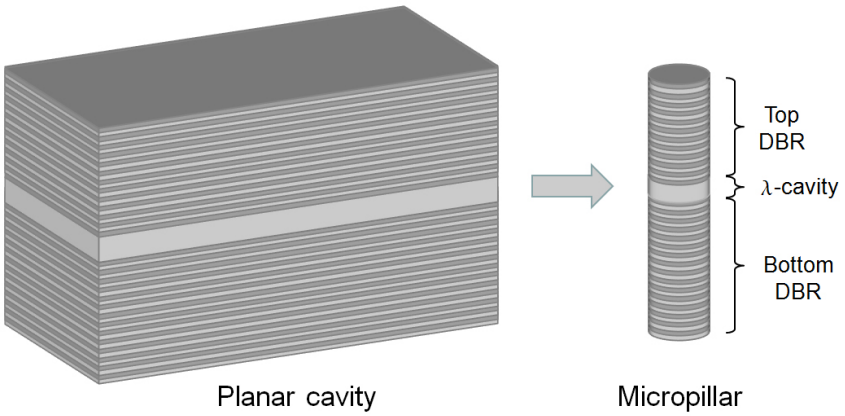

Figure 10: Drawings of a planar cavity and the pillar that can be obtained from it, from [12].

The designed structure is a simplified version of a real cavity not just because it is infinite, but also for the materials being only defined by fixed refractive indices [8]. At the same time it is important to keep in mind that no QD is modeled in this simulation, but just the cavity alone.
All the rest of the design is matching the real one. Anyway, some imperfections may still arise when the discretization is applied by the simulation. This and other issues will be thoroughly described in the following.
A summary of the theory of planar DBR cavities is given in Appendix B.

Description of the simulation setup

Due to the nature of the problem, a 2D simulation is sufficient and also saves simulation time.
To understand the issues arising from the simulation (mainly having to deal with the compromise between accuracy and time needed to simulate) it is important to describe all the pieces taking part of it. Referring to Figure 11, all of them are described briefly and their role is underlined.

- **Material design**: definition of all the layers with proper dimensions and refractive index. It acts as a background for the simulation.
- **Simulation region**: defines the area of the background material entering the simulation. In it, the space discretization (mesh) makes a sampling of the materials.
  Everything outside this region is not taking part in the computation.
- **Boundary conditions**: at each boundary, depending on the particular simulation, one can have different conditions applied to the incoming fields. In this case the boundaries crossing the structure are periodic, resulting in an infinite structure, while the top and bottom boundaries are absorbing.

[8] This is not an issue at the present level but later on it will be necessary to try to reproduce carefully the material properties.

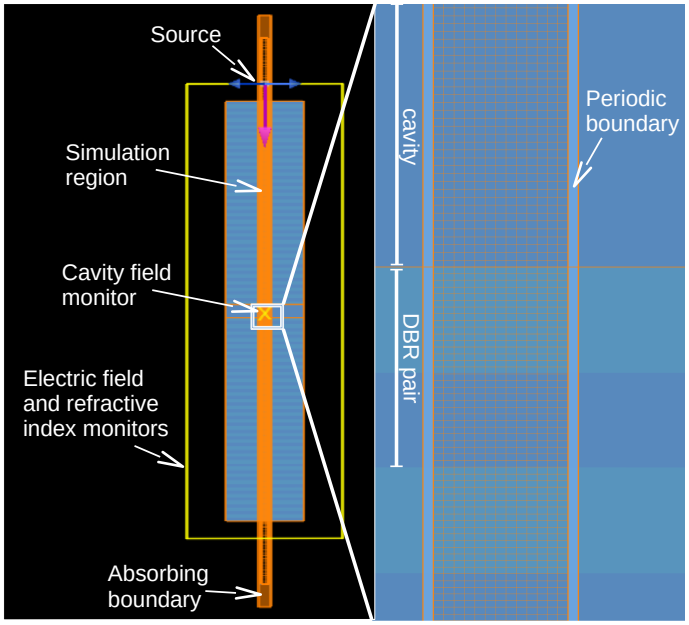

Figure 11: Descriptive picture of the simulation setup with zoom in the central region.

- **Source**: necessary to input some energy into the system, here it is a spectrally broad plane wave pulse.
- **Monitors**: lines or areas where e.g. the field evolution is recorded to be then analyzed.

Following the flow of the simulation, the source injects a pulse of light into the simulation region. The fields propagate and the resonant frequencies are trapped for some time in the cavity. Eventually, all the energy exits the system from the absorbing boundaries. In certain cases, the simulation can stop in advance. Up to that point the monitors record the fields and can reconstruct the behavior in frequency by Fourier transforming the signal in time. This approach is very useful because with a single simulation the broadband behavior is obtained.

Analysis of the simulation results

Once the simulation is completed, different quantities of interest can be extracted and analysed. Possible ways to extract the quality factor are described after checking that the simulation has correctly ended. This is done qualitatively by looking at the refractive index and the modulus of the field intensity at the resonant frequency. In particular, the results shown in Figure 12a confirm that the refractive index matches with the designed one. Even if that seems trivial, inaccurate meshing or overlapping/misplaced objects can result in an unwanted structure.
Additionally, from Figure 12b one can observe that the resonant field spends most of the time inside the cavity and penetrates (as expected) into the DBRs. Moreover near the source (left side of the figure) a higher field region is observed due to known short range instabilities inherent to the source itself.

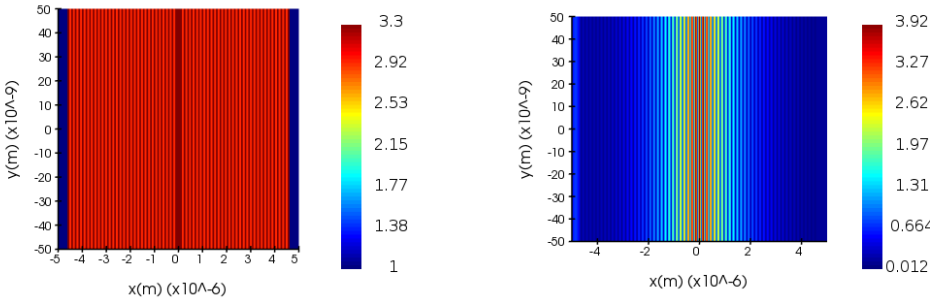

(a) refractive index (b) electric field amplitude, V/m

Figure 12: Simulation results from electric field and refractive index monitors. The view is rotated by 90° with the source placed on the left and the cavity is horizontal.

Before continuing with the discussion of the results, it is useful to remind that the simulation is not necessary to know the properties of the cavity. Vice versa, the known results are needed to test and properly set up the simulation parameters and to fix possible problems that may arise.

The goal of the simulation is to reproduce the results from the theory, in this case the resonant frequency and quality factor of the cavity (Q).
Two ways to extract the Q of the cavity from the simulation were explored.

- The first one is based on reconstructing the full reflectivity and transmission spectra and exploiting the fact that Q is the ratio of the resonance frequency and the linewidth of the peak, in formula

$$Q = \frac{\nu_{res}}{FWHM}$$

  This is done by placing a monitor that records the field that gets reflected by the cavity and one recording what is instead transmitted. The reflectivity and transmission spectra are found by performing a Fourier transform of the field arriving in time to the respective monitors.
  A serious limitation of this approach is the severe increase of the simulation time with the Q of the designed structure.

  The lifetime of a photon in the cavity is

$$\tau = \frac{Q}{2\pi\nu_{res}}$$

  consequently the width observed in the reflectivity dip (Figure 13) is limited by the simulation time if not much larger than the lifetime. The oscillations in the frequency domain data are also caused by early termination of the simulation. These ripples are the result of the convolution between the true response of the system and a sinc function. The convolution causes frequency mixing with great impact on the accuracy of the simulation.

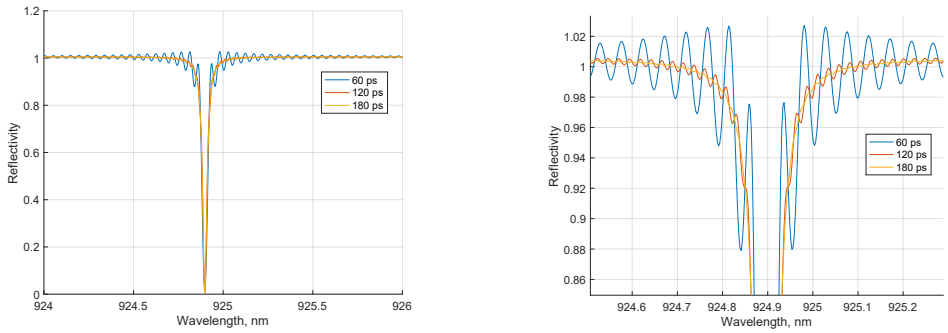

(a) full figure (b) close up

Figure 13: Reflectivity spectrum for different simulation times. The inaccuracies not described in the text are due to other parameters not being optimized (like the mesh size inside and outside the structure).

- The second approach is based on observing the way the field decays inside the cavity (Figure 14), that is strictly linked to the lifetime of the photons in it. In formula

$$Q = \frac{-2\pi\nu_{res}\log_{10}(e)}{2m}$$

where m is the slope of the envelope of the decaying field and e is the Euler's number.
This method has the great advantage of requiring much less time to simulate, but the information is limited to Q and λ_{res}.

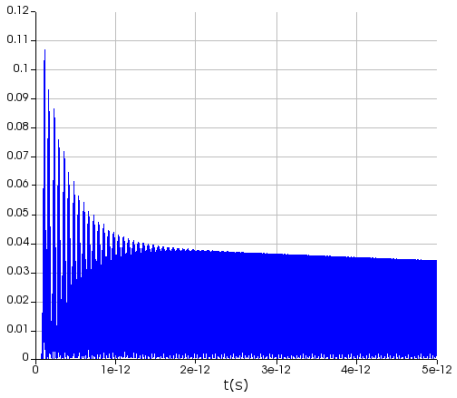

Figure 14: Electric field (V/m) decay inside the planar cavity, the interesting part to compute the Q is for $t > 2\ ps$.

At the beginning of the simulation one can observe a transient in which the source pulse enters the cavity and the interferences build up. This is removed from the computation by applying a filter window to the monitor.

With both techniques the computed Q-factor is within 1% from the theoretical one in the high Q-factor limit.

Convergence studies

Some convergence studies aimed at the optimization of the simulation are described in the following. At the same time they are useful to know where the computational power should be directed to. Good accuracy and limiting the time needed to run the simulation are desired.
Part of the convergence studies on the simulation time have already been shown in Figure 13.
Here the focus shifts to the impact on the accuracy of the mesh in the growth direction, that is critical in thin layered structures. This includes both the mesh size and the relative position with respect to the designed structure. In fact the simulation just probes the materials where the mesh point is, as part of the space discretization process.

The obtained results show that both the resonance wavelength and the Q are affected by how the mesh is overlapping with the designed structure, independently on the method used to compute the Q-factor.
The first results of the convergence studies show that if the mesh is uniform in the structure (so not considering its boundaries and periodicity), there is an improvement using a finer mesh. Still, more accurate results can be obtained with the same number of mesh points using a more clever meshing, namely by forcing the commensurability with the periodic layers.

To faithfully reproduce the designed cavity it is convenient to override the mesh separately in different regions of the structure, so that the interfaces are exactly sampled.
Two different mesh approaches have been used, with the goal of improving the quality of the simulation results without changing the complexity of the simulation (number of mesh points). The different approaches are sketched in Figure 15, where the accurately reproduced interfaces are highlighted for the three analyzed cases.

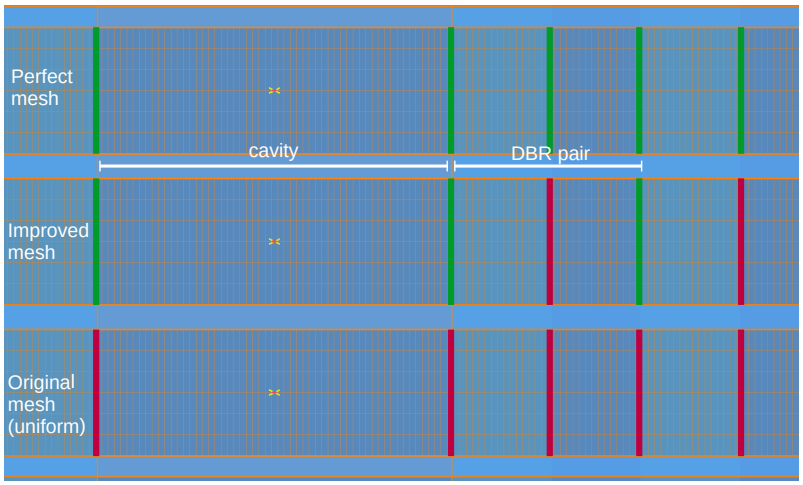

Figure 15: Descriptive picture of the meshing accuracy in reproducing the interfaces in the structure.

An issue in the definition of the mesh override is that it cannot be of the same size in the different regions. The reason is that too similar meshes are blended by the program. As a result, only some limited sets of values end up being successful.

All in all, careful definition of the mesh leads to clearly more accurate results. The trend is clear for the resonant wavelength in Figure 16. A dependence on the mesh size is still present and non-negligible even for a perfect geometry. The remaining (relatively small) errors may be caused by interpolation inaccuracies in the monitors or numerical errors in the cavity (where the field is most intense) inherent to the method.
The relative error is small (around 10^{-4}), still the improvement is remarkable just by using the intermediate approach (it is also simpler to implement).

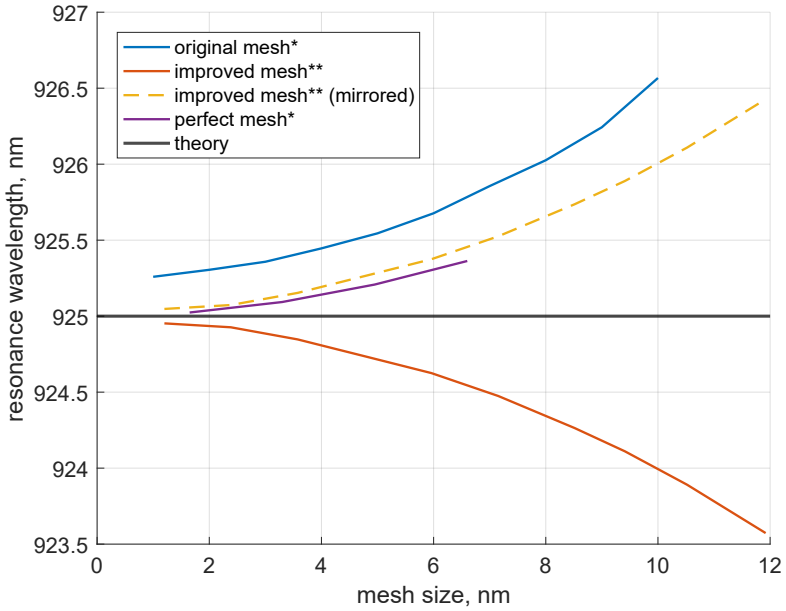

Figure 16: Summary of the convergence study as function of the mesh size.
(*: measured from the field decay; **: measured from the transmission spectrum)

With the perfectly matching mesh approach, it is possible to observe the direct effect of the mesh size, without the geometry imperfection effects. Moreover, the difference with the intermediate one can be explained theoretically using the transfer matrix method; the modeling of imperfect DBR layers is described in Appedix B. From this it was also possible to understand why there are both over- and underestimations of the resonant frequency, since this depends only on which layer is artificially made thicker.

For what concerns the Q-factor, it is also influenced by the resonant wavelength (except for too small mesh size for which the field in the cavity is poorly resolved). Other parameters can affect the accuracy of Q, like the choice of the time window and frequency range of the source. Its analysis would require a much more comprehensive multi-parameter convergence study.

As already mentioned, without further optimization the results are correct within the $\sim$1% range.

Before moving to the core of the simulation work, an idea of the complexity dependence with the mesh size (dx) is:

$$\text{2D: } Area \cdot (\lambda/dx)^3$$
$$\text{3D: } Volume \cdot (\lambda/dx)^4$$

This is only partially observed in the present simulations since the mesh was varied only in one direction.
Simulations in 3D are heavier to run, since the number of mesh points gets multiplied; the convergence testing and better meshing approaches studied so far will help in saving time and having better results.

2.2 FDTD simulation of the coupling efficiency to a fiber

After practicing on the basics of FDTD thanks to the planar cavity simulations, it is possible to face more complex problems. It is important to move from 2D to 3D to simulate real structures. The first objective is in fact to faithfully reproduce a situation similar to the one implemented in the lab. The described simulation yields some interesting results and opens the doors to many possible studies to follow.

Design

The designed structure (Figure 17) is composed of a cylindrical micropillar standing on a substrate and with a fiber core placed above it (the reasons of this choice are explained later). The micropillar is confining light laterally (by total internal reflection, as a waveguide) and vertically (thanks to 14 top and 28 bottom DBR pairs and a λ cavity between them, as in Section 2.1). The number of pairs in the top half is reduced to favor emission through the top (inspired from [10]).

The source of light is now an electric dipole mimicking the QD emission in the center of the cavity. The boundaries in the plane are no more periodic since the structure is not infinite, but they are absorbing and put sufficiently far from the materials (to not have evanescent fields reflected back).
For what concerns the simulation time, in this case the field has to fully decay to compare the transmission results. To make the simulation faster it is possible to exploit the symmetries of the structure in the plane, so the fields are computed only in one quarter of the volume and replicated in the other quadrants. Moreover the optimized meshing of the cavity has been implemented as in Section 2.1.

Preliminary results

To check that the simulation is working properly, some basic results are presented in Figure 18.

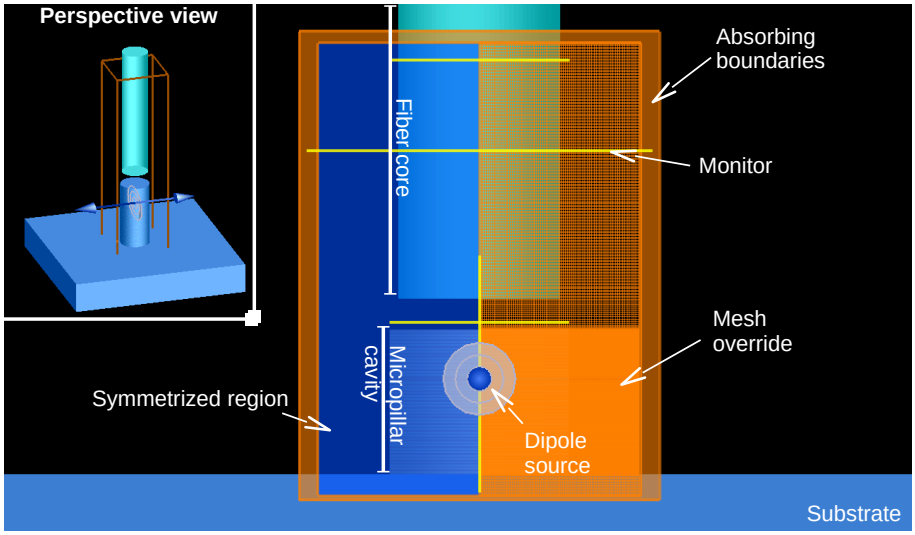

Figure 17: Descriptive picture of a section simulation setup. Inset: perspective view.

The refractive index profile assures that the structure is correctly reproduced, without problems arising from the spatial discretization. The only exception is the unavoidable staircase effect due to the pillar having a round section while the mesh is only rectangular. The induced error is very small and can be seen as a pure numerical error.
Also the field profile in the fiber is observed and it is consistent with the expected one. A slight elongation is still present along the dipole emission axis, but the fiber shapes the field as it travels.

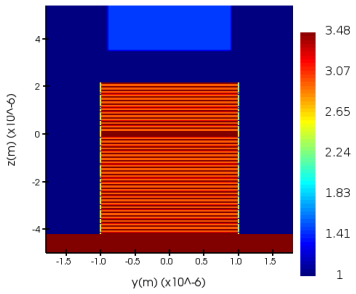

(a) Refractive index of a section of the fiber and the cavity

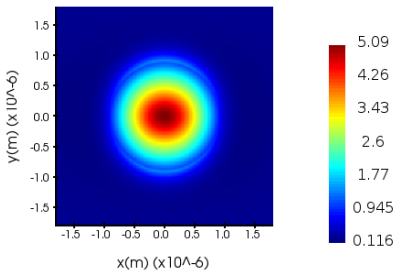

(b) Field profile after 5 μm propagation in the fiber, V/m

Figure 18: Simulation results from electric field and refractive index monitors.

Methods and analysis of the coupling efficiency

Following the flow of the simulation, the light is emitted by the dipole into the cavity and exits toward the top. After passing through a 1 μm gap in vacuum, it enters the fiber core and travels through it for more than 10 μm.

To quantify the amount of energy correctly coupled to the fiber, the chosen method consists in comparing the transmission through different monitors and the total energy emitted by the source (Figure 19a).
A renormalization is necessary because the dipole is in the cavity, thus it is subject to the Purcell effect (described in Section 1.3) and its emission is enhanced.
In Figure 19b the renormalized transmission spectra through the separation gap and the fiber are computed. Thank to both curves one can observe the gradual reduction of the coupling at the different interfaces.

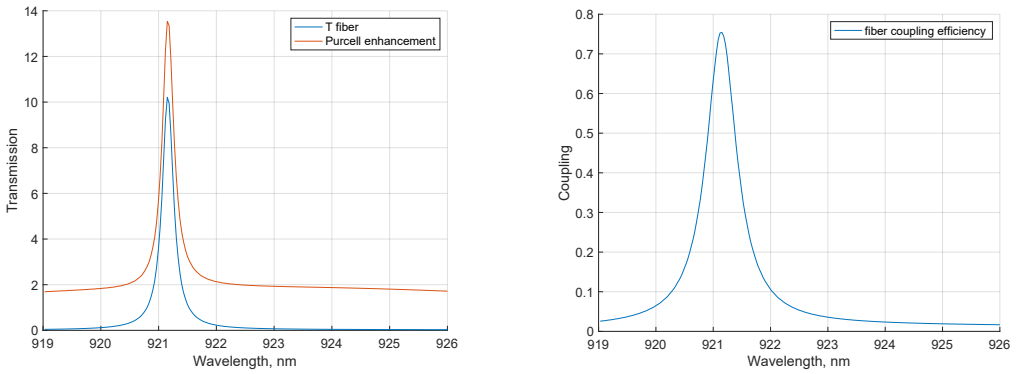

(a) Transmission spectrum in the fiber compared to Purcell enhancement.

(b) Coupling efficiency through the fiber core.

Figure 19: Analysis results of the transmission and coupling through a fiber core. The resonant wavelength of the structure is not the designed one (925 nm) due to coarse meshing to speed up the simulation.

A single value is not so significant by itself, but foreseeing a comparison with experimental results[9], with sweeps and optimization tools it will be possible to find an optimized configuration.

Fibered brightness estimation
An important parameter that can be extracted from these results is the fibered brightness. There are different parameters that take pat of it, among them the source enhanced and preferencial emission toward the top and the coupling efficiency to the fiber. In the simulation, the fiber coupling efficiency is already including all the losses at once, thus at the resonance frequency (from Figure 19b) one can extract a fibered brightness of 0.753.
Following the steps of the process, here are described the different causes of brightness reduction.

- Since the excitation of the QD is not modeled in this simulation, the efficiency is assumed to be unitary.
- The preferencial emission into the mode of the cavity is quantified theoretically by the ratio $\frac{F_p}{1+F_p}$.

[9]There is also a possibility of comparison with theoretical results overlapping the modes of the pillar and of the fiber and with far field projections.

- the out-coupling through the top DBR can be naively assumed equal to 1 (because of the unbalance in the number of top and bottom pairs). In general it is included as out-coupling efficiency η_{out}.
- The coupling of the emitted field profile into the fiber η_{fib} is given by the fraction of light that enters the fiber and is reshaped into its mode.

The overall result is obtained using the formula adapted from [10]

$$\frac{F_p}{1+F_p} \cdot \eta_{out} \cdot \eta_{fib}$$

Knowing both the Purcell factor and the fibered brightness from the simulation, one can go backward and retrieve the single parameters.
The results of the calulation are (with F_p from Figure 19a) $\frac{F_p}{1+F_p} \simeq 0.93$ and inverting the formula of the brightness $\eta_{out} \cdot \eta_{fib} \simeq 0.81$. For a more precise diagnosis of the losses, the contributions of η_{out} and η_{fib} should be splitted, to be furtherly analyzed.

Improvements in the simulation setup

The simulation can be improved in many ways. The first and most evident is adding the cladding of the fiber. Some care is needed in choosing a correct width for the simulation to not cut the field in the fiber. At the same time including more cladding the simulation time increases severely.
To faithfully reproduce the real structure, the material definition (both in the cavity and the fiber) can be improved by using experimental data. The refractive index will be dependent on wavelength and the internal losses will be automatically included in the simulation.
Another aspect to be analyzed further is the length of the fiber. For this, a compromise has to be found between the volume of the simulation and the correct expulsion of the non-guided modes in the fiber.

The simulations can be sped up by reducing the DBR pairs on top of the cavity, thus reducing significantly the Q. Some testing will be necessary to ensure that the results are not affected by this choice. This practical improvement is expected to allow convergence studies and optimization sweeps, while at present a single simulation takes ∼8-12 h to complete.

An idea of what can be achieved with this kind of simulations can be found in the literature for the fiber coupling [13] and for structure optimization in general [14].

In conclusion, the simulations of the coupling of a single-photon source to a fiber give reasonable results. After a proper evaluation it will be possible to use them to improve the fibered collection setup in the lab. Some examples are the study of the effect of the vacuum gap, the sensitivity to tilting and horizontal displacement, the effect of the numerical aperture of the fiber, and more.
Moreover the simulations are easily scalable to different wavelengths range in view of what is described in the next section.

3 Engineering QD microcavities for telecom single-photon sources

What follows is a bibliographic research for the modification of the present single-photon sources, aimed to move the emission wavelength toward the telecom range.

Long-distance quantum communication and computation are based on the exchange of information using photons as flying qubits. For the implementation of quantum networks and relays, photons must be able to propagate over long distances with the least possible interaction with matter.

There are two issues linked with the propagation of photons in fibers: losses and dispersion. Losses are linked to the absorption of particular wavelengths by the material. Dispersion during the photon propagation is the consequence of the refractive index dependence on the wavelength, thus the propagation velocity vary with it and photon wavepackets get modified. As a result the propagation for long distances into fibers affects the capability of two photons to interfere and therefore has an impact on the success rate of the quantum operation.
To fulfill both the requirements of low losses and low dispersion, new techniques to modify the present single-photon sources are needed, with the aim of adapting them to the telecom range. In particular there are two windows around 1310 nm (O-band, no dispersion and low attenuation of 0.3 dB/km) and 1550 nm (C-band, low dispersion and lowest attenuation of 0.15 dB/km)[10]; Figure 20 offers a clearer view and some hints of the causes of losses.

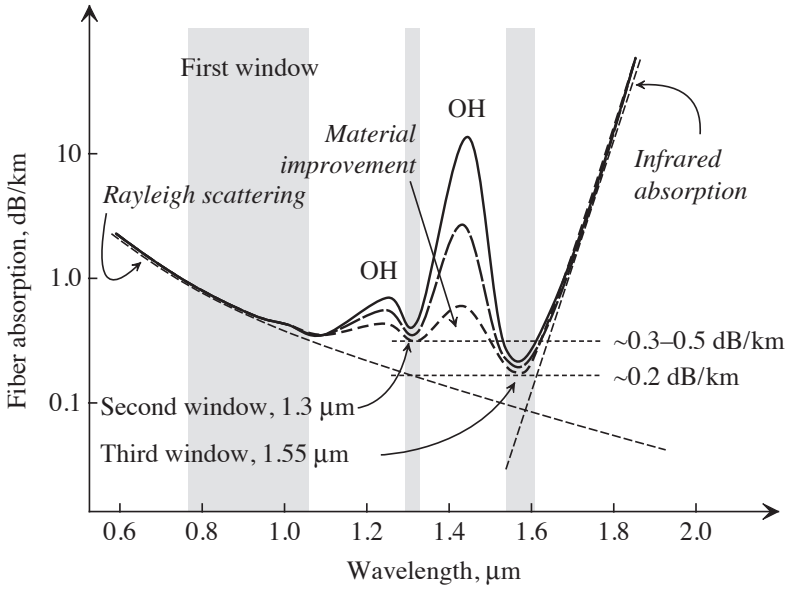

Figure 20: Absorption profile of a glass fiber, from [15]

[10]For comparison, the losses of visible photons in fibers are of the order of 3 dB/km. Intuitively the brightness of any source would be wasted if sent into a lossy channel.

A little detour is needed to understand the possible solutions, focusing on fundamental aspects impacting the choice of the materials. Not only the QD material is important but so are its surroundings and (indirectly) also the substrate.

3.1 Digression on the effect of semiconductor alloys composition on lattice parameter and bandgap [15, 16]

In general, when growing the considered III-V semiconductors compounds and their alloys in the form of thin layers one on top of the other, the lattice parameter must be almost exactly matched. Otherwise stresses build up making flat layers collapse[11]. The use of GaAs substrates is important from a technological point of view since it allows exploiting the high refractive index contrast between AlAs/GaAs layers, enabling the implementation of highly effective DBRs.

Another aspect of interest is the bandgap of the semiconductors. The emitted photon by the QD upon excitation has an energy that, due to the nanometric features of the quantum dot, is not simply given by the energy difference between conduction and valence band. Anyway a few useful qualitative remarks can be made from Figure 21.

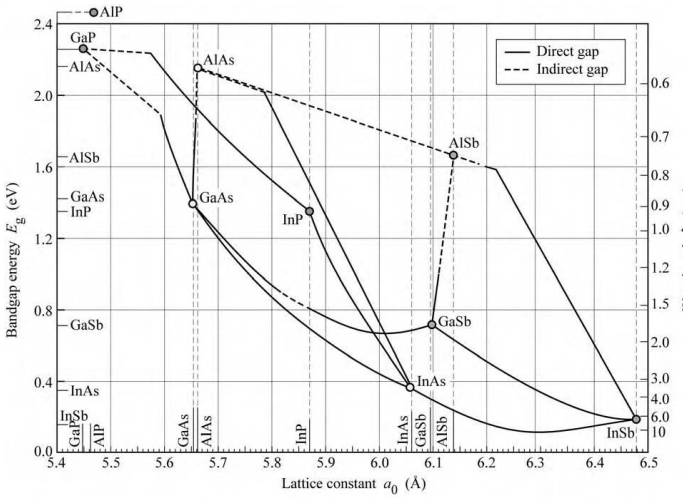

Figure 21: Bandgap energy and lattice constant of different III-V semiconductors at room temperature. Semiconductor compounds are represented by dots, lines connecting them are ternary alloys, and areas inside those lines are quaternary alloys.

Making an alloy of two or three semiconductors introduces a certain tunability in the properties, that gradually change with the relative composition. As explained previously, the two properties of interest being the lattice constant and energy gap.

[11] This phenomenon is the one that makes the self-assembly of the QDs possible in the way it is described in Section 1.3

Since the lattice-matching condition must be satisfied for a successful growth, this translates into using materials lying on the same vertical line. To choose the emission, the alloy composition can be tuned to match the desired window, limiting the choice to horizontal cuts.

A more detailed analysis of Figure 21 is not needed since the two described properties (lattice constant and bandgap) are strictly linked only in solid semiconductors. To have the complete picture of the studied case, it is necessary to consider that QDs are confined inside larger gap materials and are stressed by the difference in lattice constant with their surroundings.
Confinement results in more distance in energy between occupied and unoccupied states alongside with discretization of the levels. In QD the stress from the environment can furtherly modify the dimension of the QD and in turn its emission (in general tensile strain). Moreover there is a change in the energy splitting between heavy holes and light holes[12] that may complicate the picture.
Thanks to these concepts, one can understand how and why the different solutions are adopted to shift the emission of semiconductor QDs in microstructures toward telecom wavelength.

3.2 Possible solutions for the design of QD telecom single-photon sources [16, 17]

The current sources emit around 930 nm. In order to shift their emission wavelength toward the telecom range it is either possible to increase the size of the semiconductor QDs by itself or to reduce the lattice mismatch between the QDs and the surrounding materials.

A list of some of the strategies to emit at lower energy is presented, with a few comments about the possible issues related to that particular solution.
Each solution starts with all the rest of the structure unmodified as it is described in chapter 1.3. To summarize, the source was made of InAs QD in between of a GaAs λ cavity, surrounded vertically by alternating AlAs/GaAs $\lambda/4$ layers. The focus is on the cavity and QD material since these are affecting the emission wavelength, but the compatibility with the substrate sets some additional limitations.

Some options are:

- deposition of InGaAs stress reducing layer (SRL) on InAs QD instead of directly GaAs. This technique, other than relieving the compressive strain on the QD, also reduces inter-diffusion of gallium and indium atoms in QDs and surrounding material, and results in a larger QD size.

- growth of InAs QD on a metamorphic buffer layer with increasing In content moving from the DBR to the wetting layer, with smaller lattice mismatch close

[12] In nanostructures the two bands are already not degenerate due to confinement.

to the top. In other words the buffer layer links gradually the lattice of bottom DBR to the intrinsic one of QD.

- use of InGaAs QD instead of InAs. Even if Ga has smaller lattice constant (so it may seem counterintuitive) the reduced strain in the end results in larger QDs.
- use of InP substrate, with comparably low lattice mismatch (thus less strain) allowing the growth of larger and less strained InAs islands. The downside is that InP substrates are brittle and expensive, and there is a lack of lattice-matched DBR materials with high refractive index contrast to build efficient cavities to surround the QD.

Not all the described options allow to reach 1550 nm up to now.
Some of them can also be combined, when the technology is compatible, for an improved effect.

In conclusion, this bibliographic work is intended to understand the possible paths that can be taken to build a telecom single-photon source, while learning about the underlying physical processes. This is the first step in the direction of the design of single-photon sources in the telecom range. A more detailed analysis of the pros and cons of each approach will be needed to choose which one to implement.

4 Conclusions and prospects

In conclusion, the internship was very useful to learn and practice with the technology used by the group. The experimental part have been strongly limited by the current situation, but I had the opportunity to learn how to simulate microcavities and other structures with a commercial software.
All the work was improved by collaborating with the team in Quandela and with the group of Pascale Senellart in C2N.

The work carried out during the internship opens different continuation paths as part of the PhD that will follow.
In the short term, the simulations of the coupling of the single-photon source with a fiber can be improved. An important step forward will be to compare the obtained results with theory and experimental results. This will be possible to the current direction in which the excitation/collection setup is taking, that is to reduce as much as possible the free-space propagation of light by reaching the source directly with a high-NA fiber. Hopefully, an agreement of the simulations with the experiments will be set. Once the validity of the simulation is checked, it will be possible to predict potential downsides and run optimization sweeps.

The long term perspective is to work on the design and realization of a single-photon source in the telecom wavelength starting from the present successful technology.
The approach to the design of telecom single-photon sources (interesting for their compatibility with long-distance fiber communications) consists in understanding the present ones and identifying the technological changes and challenges that will be faced. Different approaches are already under study.
The plan is to move step by step toward the final goal of 1550 nm (lowest loss telecom window). Two interesting intermediate wavelengths are 1064 nm (used in free space optical communicationsand reachable without changing the whole process) and 1310 nm (low-loss and dispersionless telecom window).
The multiple challenges to overcome and opportunities will be discovered along the way, in the continuation of this project.

A FDTD basics

Finite Differences Time Domain (FDTD) is a method to solve the electromagnetic wave equation in the time domain based on the finite-differences approximation. Opposed to other methods working in the frequency domain, the time domain feature of this method allows to study the field evolution in time, thus including transients. The key steps to obtain the equations to make the fields evolve in time are:

- start from the Maxwell equations linking electric and magnetic field in absence of charges, paired with the corresponding constitutive relations for isotropic materials

$$\nabla \times \vec{E} = -\frac{\partial \vec{B}}{\partial t};\ \vec{H} = \frac{1}{\mu}\vec{B}$$

$$\nabla \times \vec{H} = \frac{\partial \vec{D}}{\partial t};\ \vec{D} = \varepsilon \vec{E}$$

- isolate the time derivatives

$$\frac{\partial \vec{H}}{\partial t} = -\frac{1}{\mu}\,\nabla \times \vec{E}$$

$$\frac{\partial \vec{E}}{\partial t} = \frac{1}{\varepsilon}\,\nabla \times \vec{H}$$

- introduce discretization: finite differences approximation in time

$$\frac{\vec{H}\left(t+\frac{\Delta t}{2}\right) - \vec{H}\left(t-\frac{\Delta t}{2}\right)}{\Delta t} = -\frac{1}{\mu}\,\nabla \times \vec{E}(t)$$

$$\frac{\vec{E}\,(t+\Delta t) - \vec{E}\,(t)}{\Delta t} = \frac{1}{\varepsilon}\,\nabla \times \vec{H}\left(t+\frac{\Delta t}{2}\right)$$

- reformulate as an update equation by separating past and future times (more stable)

$$\vec{H}\left(t+\frac{\Delta t}{2}\right) = \vec{H}\left(t-\frac{\Delta t}{2}\right) - \frac{\Delta t}{\mu}\,\nabla \times \vec{E}(t)$$

$$\vec{E}\,(t+\Delta t) = \vec{E}(t) + \frac{\Delta t}{\varepsilon}\,\nabla \times \vec{H}\left(t+\frac{\Delta t}{2}\right)$$

The fields are updated alternately every half-timestep. Also the spatial positions in which the fields are defined are shifted in what is called a Yee cell (Figure 22), useful for the optimized computation of the curl.

Moreover in each step of the cycle there are updates at the boundaries and from the source. This is essential to remove and inject energy from/in the simulation region.

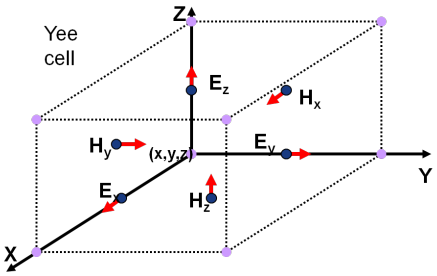

Figure 22: Yee cell with the components of the fields shown for one mesh point.

B Planar cavity theory [12]

A single DBR is made of a stack of $\lambda/4$ layers of alternating higher and lower refractive index materials. It acts as a mirror in the wavelength range it is designed for, with a characteristic stop-band around.
When a defect is introduced in the stacking (like one layer of the DBR missing/being thicker), the structure can also be seen as two DBRs separated by a spacer, making it easier to see the cavity as a Fabry-Perot interferometer.
The result in both interpretations is a dip in the reflectivity in correspondance of the designed wavelength, indicating that some modes in the stopband become sustainable. Both the described behaviors are shown in Figure 23.

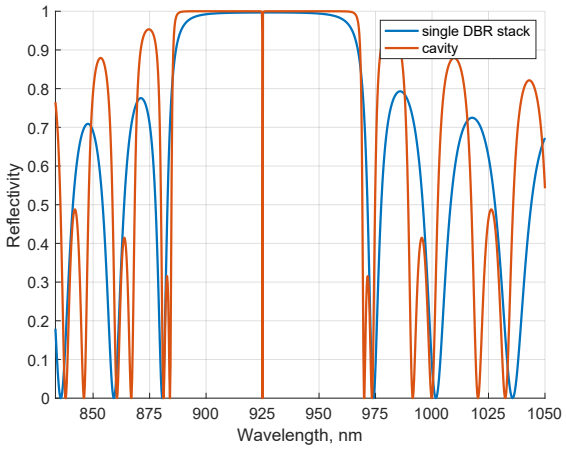

Figure 23: Reflectivity of one DBR and of the full cavity, computed by transfer matrix method

The reflectivity and transmission of the cavity can be understood in terms of destructive and constructive interferences. A more rigorous approach for calculating the properties of planar[13] multi-layer structures uses the transfer matrix method. It consists in calculating the field throughout the structure by propagating it from one layer to the other by matrix relations.
The method is well suited for generalization) for R,T from continuity requirements it follows that the transfer matrix for a system of a given number of layers is obtained by simple matrix multiplication of the matrices of single layers.

In addition to the spectrum, another important property of the cavity is the quality factor (Q), quantifying its ability to confine light. To make it more intuitive, , the full physical meaning is the comparison of the frequency at which the system oscillates with the rate at which it dissipates its energy (see main text).

Since the wavelength is dependent on the medium, the dimensions of the structure depend on the target λ_{res} and the refractive indices of the chosen materials.

[13]To be considered infinite, the dimension of the structure in the plane must be much larger than wavelength.

The structure is designed to have a resonance at 925 nm. As a consequence of choosing $n_{GaAs} = 3.3$ and $n_{AlGaAs} = 2.93$, then the dimensions of the three layers are $d_{cavity} = \lambda/n_1 = 280.30$ nm, $d_{DBR1} = \lambda/4\ n_1 = 70.08$ nm, and $d_{DBR2} = \lambda/4n_2 = 78.92$ nm. The result of the theory for the structure designed with 30 DBR pairs on both sides of a λ cavity is Q=32230. This result[14] is used as reference in the simulations of Section 2.1.

Theoretical analysis of imperfect meshing

The transfer matrix method has been used also to verify that the observations in the result analysis in Figure 16 (Section 2.1) were correct. In particular the addressed problem is to compute the exact resonant wavelength of an imperfect cavity. The imperfection is due to the mesh not exactly matching the interfaces of the layered structure, as depicted in Figure 15. The effect of the intermediate solution (in which the mesh is commensurate with the DBR periodicity) can be modeled by defining an error parameter that is added to the dimensions of one layer and subtracted from the other. A linear trend is observed in Figure 24, coherent with the observations made in the main text.

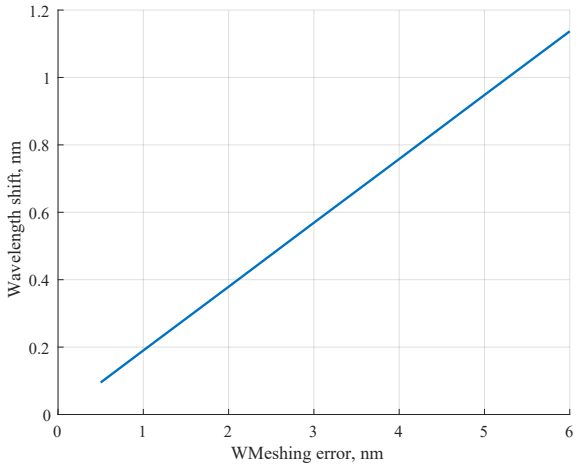

Figure 24: Theoretical computation of the effect on the resonance wavelength of the inter-DBR interface meshing error

[14] it is just a coincidence that the quality factor is close to the one in [11] since the refractive indices are not the real ones and the substrate reduces the Q.

C Data analysis

In the context of a first analysis of the sources, here are described two different measurements: LED reflectivity and photoluminescence spectroscopy (PL).
These techniques characterize the spectral properties of each source, namely its QD lines and cavity resonances. This allows to choose the sources that are, or can be, in resonance with the cavity.

During the internship the objective was to familiarize with the data analysis tools by plotting and fitting the spectra. Thanks to the first weeks spent in the lab it is also interesting to understand a few features that can be extracted from the data (or more in general during the measurement by changing some parameter in real time).

- LED reflectivity: identify the frequency of the first and successive (mainly second) modes of the cavity. A dip is observed in correspondence of its resonances. The first one (at lower energy) is found illuminating the center of the pillar, while the others by moving a bit on the sides with piezos.
  One can see the variation of the mode when the whole structure is cooled to cryogenic temperature (shift of the cavity mode to higher energy), the effect of smaller teperature variations, or the change with applied voltage.

- PL: characterization performed by sending a laser of sufficiently high frequency to excite electrons in the material. In this case the interest is both on the cavity and the QD. Excited electrons relax with the emission of a photon at a specific wavelengths that characterize the system.
  The different contributions can for example be distinguished by increasing the excitation laser power or changing the voltage. The QD lines saturate and are shifted respectively.

References

[1] Pascale Senellart, Glenn Solomon, and Andrew White. High-performance semiconductor quantum-dot single-photon sources. *Nature Nanotechnology*, 12(11):1026–1039, Nov 2017.

[2] H. Ollivier, S. E. Thomas, S. C. Wein, I. Maillette de Buy Wenniger, N. Coste, J. C. Loredo, N. Somaschi, A. Harouri, A. Lemaitre, I. Sagnes, L. Lanco, C. Simon, C. Anton, O. Krebs, and P. Senellart. Hong-ou-mandel interference with imperfect single photon sources, 2020.

[3] Peter Michler. *Quantum dots for quantum information technologies*, volume 237. Springer, 2017.

[4] Hélène Ollivier, Ilse Maillette de Buy Wenniger, Sarah Thomas, Stephen C. Wein, Abdelmounaim Harouri, Guillaume Coppola, Paul Hilaire, Clément Millet, Aristide Lemaître, Isabelle Sagnes, Olivier Krebs, Loïc Lanco, Juan C. Loredo, Carlos Antón, Niccolo Somaschi, and Pascale Senellart. Reproducibility of high-performance quantum dot single-photon sources. *ACS Photonics*, 7(4):1050–1059, 2020.

[5] Hui Wang, Yu-Ming He, T.-H. Chung, Hai Hu, Ying Yu, Si Chen, Xing Ding, M.-C. Chen, Jian Qin, Xiaoxia Yang, Run-Ze Liu, Z.-C. Duan, J.-P. Li, S. Gerhardt, K. Winkler, J. Jurkat, Lin-Jun Wang, Niels Gregersen, Yong-Heng Huo, Qing Dai, Siyuan Yu, Sven Höfling, Chao-Yang Lu, and Jian-Wei Pan. Towards optimal single-photon sources from polarized microcavities. *Nature Photonics*, 13(11):770–775, Nov 2019.

[6] O. Gazzano, S. Michaelis de Vasconcellos, C. Arnold, A. Nowak, E. Galopin, I. Sagnes, L. Lanco, A. Lemaître, and P. Senellart. Bright solid-state sources of indistinguishable single photons. *Nature Communications*, 4(1):1425, Feb 2013.

[7] Xu Wang, Lei Xu, Yun Jiang, Zhouyang Yin, Christopher C. S. Chan, Chaoyong Deng, and Robert A. Taylor. III–v compounds as single photon emitters. *Journal of Semiconductors*, 40(7):071906, jul 2019.

[8] Lorenzo de Santis. *Single photon generation and manipulation with semiconductor quantum dot devices*. Theses, Université Paris-Saclay, March 2018.

[9] Pascale Senellart, Valérian Giesz, and Loic Lanco. Ultrabright single-photon sources. *Photoniques*, pages 23–26, 2017.

[10] N. Somaschi, V. Giesz, L. De Santis, J. C. Loredo, M. P. Almeida, G. Hornecker, S. L. Portalupi, T. Grange, C. Antón, J. Demory, C. Gómez, I. Sagnes, N. D. Lanzillotti-Kimura, A. Lemaítre, A. Auffeves, A. G. White, L. Lanco, and P. Senellart. Near-optimal single-photon sources in the solid state. *Nature Photonics*, 10(5):340–345, May 2016.

[11] A. K. Nowak, S. L. Portalupi, V. Giesz, O. Gazzano, C. Dal Savio, P.-F. Braun, K. Karrai, C. Arnold, L. Lanco, I. Sagnes, A. Lemaître, and P. Senellart. Deterministic and electrically tunable bright single-photon source. *Nature Communications*, 5(1):3240, Feb 2014.

[12] Adrien Dousse. Deterministic cavity-quantum dot coupling and fabrication of an ultrabright source of entangled photon pairs. 2010.

[13] Ben Ma, Ze-Sheng Chen, Si-Hang Wei, Xiang-Jun Shang, Hai-Qiao Ni, and Zhi-Chuan Niu. Single photon extraction from self-assembled quantum dots via stable fiber array coupling. *Applied Physics Letters*, 110(14):142104, 2017.

[14] Paweł Mrowiński and Grzegorz Sęk. Modelling the enhancement of spectrally broadband extraction efficiency of emission from single inas/inp quantum dots at telecommunication wavelengths. *Physica B: Condensed Matter*, 562:141 – 147, 2019.

[15] Giovanni Ghione. *Semiconductors, alloys, heterostructures*, page 1–51. Cambridge University Press, 2009.

[16] Simone Luca Portalupi, Michael Jetter, and Peter Michler. InAs quantum dots grown on metamorphic buffers as non-classical light sources at telecom c-band: a review. *Semiconductor Science and Technology*, 34(5):053001, apr 2019.

[17] Xin Cao, Michael Zopf, and Fei Ding. Telecom wavelength single photon sources. *Journal of Semiconductors*, 40(7):071901, jul 2019.